

## DIAGNOSTIC MEASUREMENTS IN RF PLASMAS FOR MATERIALS PROCESSING

J. R. Roberts, , J. K. Olthoff,  
M. A. Sobolewski, R. J. Van Brunt, and J. R. Whetstone  
National Institute of Standards and Technology  
Gaithersburg, Maryland 20899

S. Djurović  
Institute of Physics, Novi Sad,  
Trg Dositeja Obradovića 4, 21000 Novi Sad, Yugoslavia

### ABSTRACT

Radio frequency (rf) plasmas are utilized in many applications in materials processing, such as semiconductor fabrication, surface modification, and coating. Plasma processing has replaced older techniques, such as wet chemistry, because the latter could not provide the necessary characteristics as process demands increased. A good example of this is the reduction of the feature size in semiconductors. The present critical dimension for semiconductor processing is  $0.8 \mu\text{m}$  and is anticipated to be  $\leq 0.25 \mu\text{m}$  by the year 2000. At present only plasma processing exhibits the potential of producing these line widths.

An important factor, as the demands on the processing of materials become more critical, is exactly how to determine that the plasma is actually performing the process as designed. One way that is being investigated is to design control diagnostics that necessarily operate in real-time, *in situ*, without significantly perturbing the process. Many such diagnostic methods have been proposed and are vigorously being investigated. They include probing the plasma with lasers, electric and mass selecting probes, and by observing the emission of radiation coming from the plasma. All of these and others must be investigated if the demands of material processing are to be met. Some of the methods being investigated for process control diagnostics are presented.

### I. INTRODUCTION

The use of various kinds of metrology to set the conditions of a complicated machine has been a goal of every manufacturer. For production line devices that utilize plasmas to process materials, such as semiconductor etchers, the norm has been to measure the applied voltage or power, the gas pressure, its constituency and flow rate. It has been observed<sup>1</sup> that this is not sufficient to guarantee the day-to-day reproducibility of the desired process or to match one "identical" process machine to another. Since the requirements on these process machines are becoming more and more demanding, e.g. with the decrease in feature size in semiconductors and the increase in throughput, it is necessary to find a set of process control measurements that will suit this new demand.

The purpose of the experiments described here is to investigate various measurements as diagnostics that are sensitive to plasma conditions, particularly changes in the electron and ion energy distributions that might find application in process controls. Since the free electrons in a plasma are primarily responsible for the

population of excited states in atoms and ions, as well as the ionization of the atoms, one purpose of these experiments is to measure certain excited state populations (or population ratios) that are sensitive to changes in the electron energy distribution. Since the ion kinetic energy affects the reactions at the plasma/surface interface, a second purpose of this work is to measure correlations between changes in plasma parameters and the ion kinetic-energy distributions in the plasma.

The Gaseous Electronics Conference (GEC) RF Reference Cell<sup>1</sup> was chosen as the experimental platform because its plasma and electrical characteristics are being thoroughly studied at many laboratories throughout the U.S. Temporally and spatially resolved spectroscopy was chosen as the method to measure the optical emission from the plasma. This method is non-intrusive and has proven to be a successful diagnostic method for the investigation of plasma conditions. Energy analyzing mass spectrometry was chosen to measure ion energy distributions.

Mixtures of argon and helium were chosen to be the gases for the optical emission measurements because they will not react with each other or the plasma chamber producing unknown processes that could affect the interpretation of the experimental results. Also, since there exist a great deal of atomic data on these elements, such as emission wavelengths, transition probabilities and excitation cross sections, the experimental results are easier to interpret. The experimental conditions that were chosen were the same as the reference conditions of the Reference Cell (see Ref. 1). Previous work done by all the laboratories indicates that these were the conditions where the plasma was most stable and reproducible. The plasma parameters of the temperature and density for the electrons, ions, and atoms are expected to be in the range of similar plasmas.<sup>2</sup> For the mass spectrometry studies, argon was chosen because of the relatively simple chemistry involved in the discharge, the large amount of previous research done on argon plasmas, and the existence of a reasonably reliable set of cross section data.

Neutral helium triplet and singlet optical emission lines arising from the upper states 3p, 3d, 4s, 4p, and 4d were observed. The ratios of the triplet-to-singlet line intensities were recorded with changes in pressure and percentage of Ar in He. Radial scans of the plasma emission from argon lines were also observed. From these observations radial profiles of the relative populations of Ar excited states were deduced. Temporally resolved optical emission of Ar and Ar<sup>+</sup> were also observed as a function of pressure and distance from the powered electrode. The mass spectra reported here are for Ar<sup>+</sup> and Ar<sub>2</sub><sup>+</sup> utilizing the energy analyzing mass spectrometer. These observations were recorded as a function of probe position.

## II. EXPERIMENTAL DESCRIPTION

### A. Plasma Source

The experimental arrangement is schematically described in Figure 1. The GEC RF Reference Cell is a parallel plate discharge chamber with 102 mm electrodes separated by 25 mm. They are cylindrically symmetric and their surfaces are horizontal. The top electrode has 169 holes with a diameter of 380  $\mu\text{m}$  to provide a showerhead gas inlet and is grounded to the chamber on the outside of the vacuum interface. The bottom electrode is powered by a 13.56 MHz rf power supply with a capacitively coupled matching network. Flow rates were 20 standard cubic centimeters per minute (sccm) and peak-to-peak voltages ranged from 40-200 V at a frequency of 13.56 MHz.

The cylindrical vacuum chamber is constructed of stainless steel and has 8 radially-looking side ports at the chamber midplane. Two of the ports are fitted with 136 mm diameter quartz windows for the spectroscopic observations. Two ports orthogonal to these are 152 mm conflat flanges to accommodate a turbomolecular pump and the radially translating probe tip of the mass spectrometer. Four 70 mm conflat flange ports at 45° with respect to the other 4 ports have mounted pressure transducers and an electric probe, which can be inserted into the plasma at its midplane.

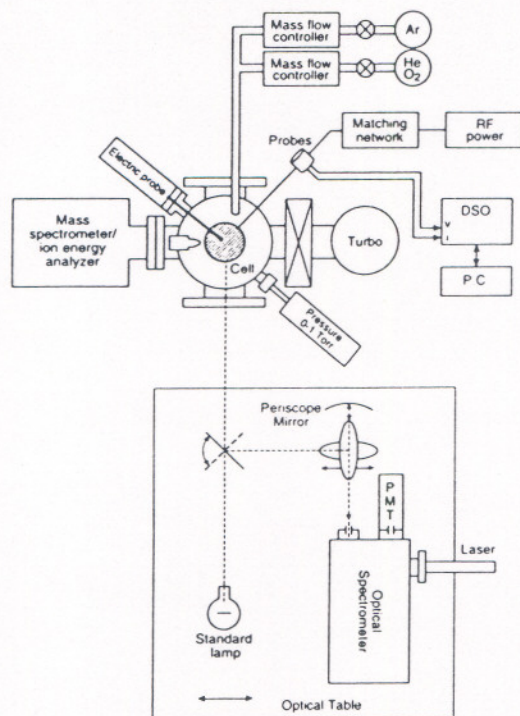


Figure 1. Schematic of experimental setup showing the Reference Cell, the energy analyzing mass spectrometer, electric probe, pressure gauge, gas flow control, power supply and matching network. Also shown is the optical spectrometer, reflecting periscope imaging optics, standard lamp, and components which are moved to scan emission profiles.

### B. Optical Emission Measurements

The spectroscopic apparatus consists of a 2/3 m Czerny-Turner type grating spectrometer. This spectrometer is equipped with a cooled Burle<sup>\*</sup> C31034A photomultiplier for detection of the emission signal. Both pulse counting and current mode observations were made. The pulse counting technique, using a time-to-amplitude-converter (TAC) and a multichannel-analyzer (MCA), was used for the temporally resolved measurements and is schematically shown in Figure 2. For current mode operation a picoammeter is substituted for the pulse counting acquisition system. The spectrometer is equipped with a retractable mirror near its exit slit so a He-Ne laser may be substituted for the detector for alignment purposes. The vertical spectrometer entrance and exit slits are typically 150  $\mu\text{m}$  wide and 2 mm high. The optics to image the plasma onto the spectrometer slit are front surface mirrors with

coatings to efficiently reflect the plasma emission at wavelengths from 200 nm to 1500 nm. There are three flat mirrors and one concave mirror, each 152 mm in diameter. The concave mirror (650 mm focal length) is positioned so the plasma image is demagnified onto the entrance slit by approximately a factor of 2. These mirrors are arranged to act as a periscope bringing the level of the plasma emission to the same height as the spectrometer, as well as rotating the image of the plasma by 90°. By this rotation, the electrode surfaces are imaged parallel to the long dimension of the entrance slit, thus permitting observations close to the electrode surface as well as providing the highest possible spatial resolution of the plasma to be observed. The spatial resolution was  $\sim 0.5$  mm vertically and  $\sim 4$  mm horizontally. Because of the periscope, scanning of the plasma emission between the electrodes can be accomplished by translating one of the mirrors (see Figure 1). Translating the table permits horizontal scans of the plasma and an Abel inversion calculation<sup>3,4</sup> is performed to convert the horizontal emission profile into a radially symmetric distribution of the plasma emission. This process is necessary if real spatial distributions are to be interpreted. A calibrated tungsten filament lamp is mounted on the optics table and is substituted for the plasma source by rotating one of the flat mirrors (see Figure 1). This lamp is used to calibrate the optics/spectrometer system to obtain absolute spectral radiance measurements.

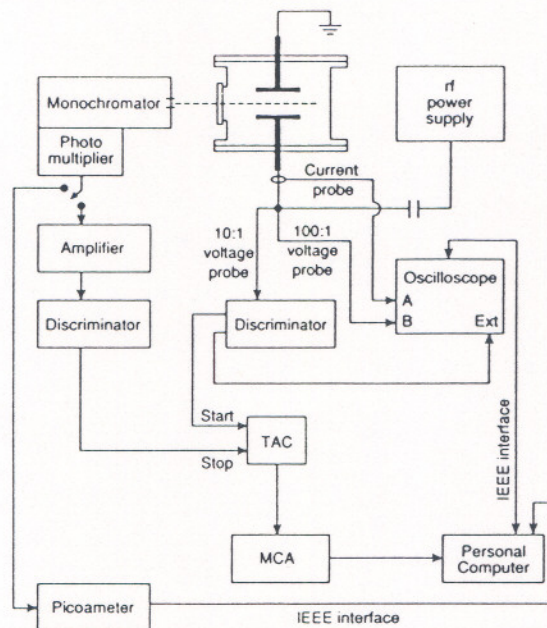


Figure 2. Schematic diagram showing optical emission data acquisition systems. The temporally resolved measurements are accomplished with a pulse counting technique utilizing the TAC-MCA and digital oscilloscope recording via an IEEE interface to a personal computer. The time-integrated measurements are done substituting a picoameter.

### C. Energy Analyzed Mass Spectrometer

The mass spectrometer apparatus is a VG Instruments\*, SXP300-CMA system which consists of a cylindrical mirror ion-energy analyzer<sup>5</sup> coupled to a 300 atomic mass

unit (AMU) quadrupole mass spectrometer. Ions are sampled via a 200  $\mu\text{m}$  aperture through a grounded stainless steel cone into the differentially pumped region of the analyzer. The orientation of the analyzer and sampling orifice with respect to the cell electrodes is shown in Figure 3.

Note that ions are sampled from the side of the plasma and not through an electrode as is common in other experiments.<sup>6-8</sup> This configuration is thought to be closer to the geometry which would be employed if this diagnostic were installed in a commercial etching reactor. The ion-energy analyzer and mass spectrometer may be moved by means of a bellows assembly so the distance from the sampling orifice to the edge of the electrode assembly may be varied from 0-10 cm. Ion kinetic energy distributions are obtained by selecting a particular mass from the spectrometer and then scanning the energy of the ions entering the energy analyzer. An energy resolution of 0.5 eV is maintained over the entire energy range scanned. Adjustments to the ion energy scale to correct for surface charging effects in the sampling cone are made based upon the observed kinetic-energy threshold for  $\text{Ar}^+$  detection from an argon discharge.

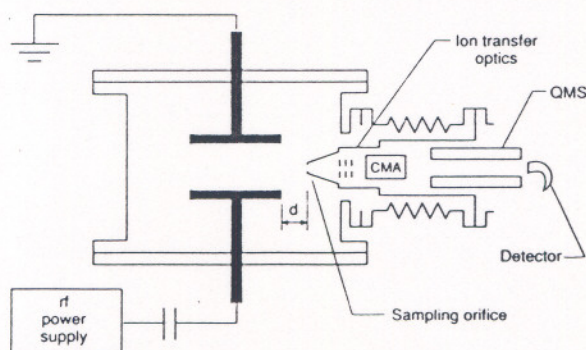


Figure 3. Schematic diagram showing the orientation of the ion-energy analyzer and mass spectrometer with respect to the Reference Cell electrodes. The distance from the edge of the electrode assembly to the aperture is  $d$ , the sampling orifice is a 200  $\mu\text{m}$ , CMA is the cylindrical mirror ion-energy analyzer, QMS is the quadrupole mass spectrometer.

### III. EXPERIMENTAL OBSERVATIONS

#### A. Optical Emission Measurements of He Triplet/Singlet Ratios

We observed emission from both the triplet and singlet lines of neutral helium. Triplet-to-singlet emission line ratios can be used to investigate the effect of the electron energy distribution on the excitation function.<sup>9</sup> The levels and the observed emission wavelengths in this experiment are shown in Figure 4. Transitions to the  $1s$   $^1\text{S}$  ground state were not observed. The metastable  $2s$   $^3\text{S}$  state of the He atom acts as the ground state for the triplet system. The population of excited states making transitions to the ground state and to this metastable level may exhibit radiation trapping effects. Therefore, a model of the excited state population is necessary to interpret emission intensities.<sup>9</sup> A detailed analysis may not be so important, however, if one only desires information concerning the temporally and spatially dependent electron energy distribution in the plasma, since some emission lines are more sensitive to changes in the electron energy distribution than others.

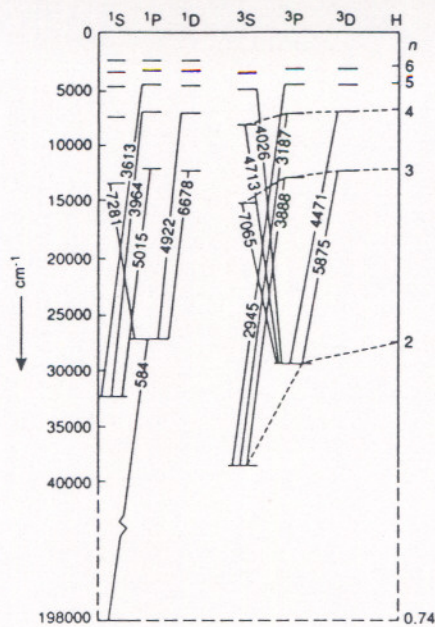


Figure 4. Grotrian diagram of He, with terms of H for comparison. Wavelengths are in Å. (H. G. Kuhn, *Atomic Spectra*, Academic Press, New York, 1962, p. 131).

Figures 5 and 6 show examples of the ratios of the triplet-to-singlet lines observed in this experiment as a function of pressure and percent of Ar admixed in He. Table I gives the correspondence between the upper state 3s, 3p, 4s, 4p and 4d and the line wavelengths in nm and their respective triplet and singlet designation (see Figure 4).

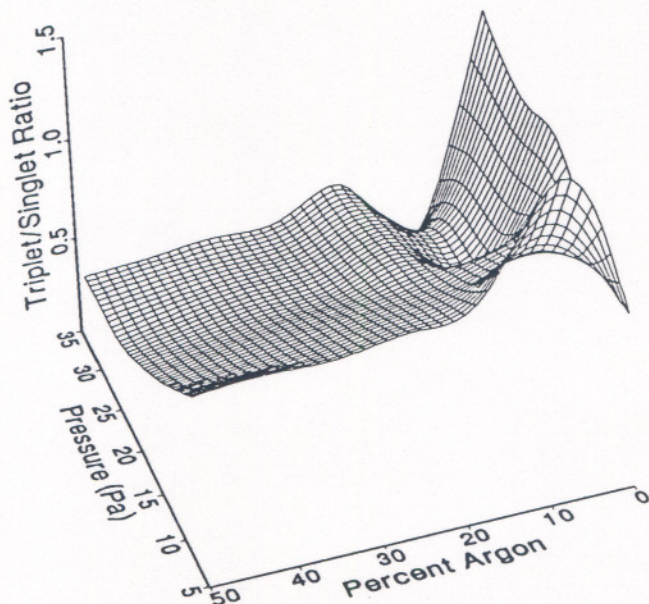


Figure 5. Optical emission measurements of the He 3p triplet-to-singlet ratio as a function of percent Ar in He and different pressures.

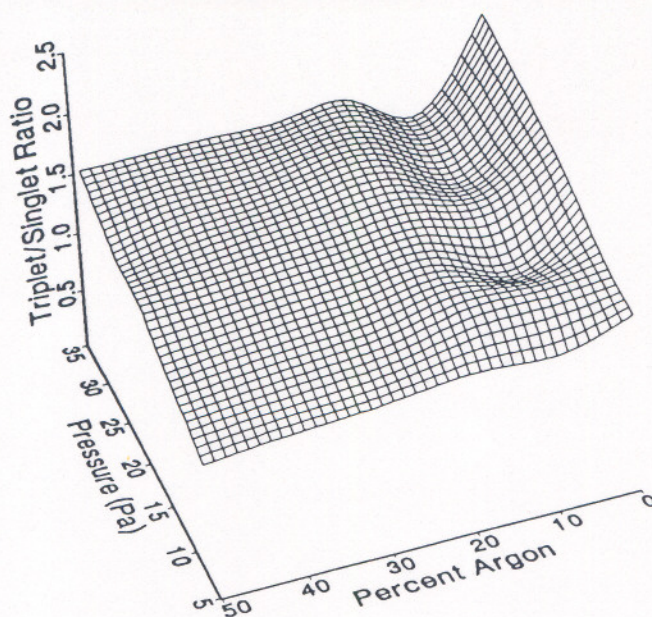


Figure 6. Optical emission measurements of the He 4d triplet-to-singlet ratio as a function of percent Ar in He and different pressures.

Table I Wavelengths (nm) and designations of measured He line ratios

3s	3p	4s	4p	4d
$\lambda 706.5(^3S)$	$\lambda 388.9(^3P)$	$\lambda 471.3(^3S)$	$\lambda 318.7(^3P)$	$\lambda 447.1(^3D)$
$\lambda 728.1(^1S)$	$\lambda 501.5(^1P)$	$\lambda 504.7(^1S)$	$\lambda 396.4(^1P)$	$\lambda 492.1(^1D)$

The observations of these He lines were taken over a range of pressures and admixtures of Ar. The pressures were: 6.67, 10.00, 13.33, 20.00, 26.66, and 33.33 Pascals (133.322 Pa/Torr). The percent of Ar in the total was: 0, 10, 25 and 50.

Since the ionization potential of Ar is much smaller than that of He, one expects small admixtures of Ar to perturb the conditions of the plasma. This can be seen by the gradients in the triplet-to-single ratio, especially for the 3p ratios (Figure 5). Because the population of the triplets and singlets are essentially two relatively independent systems in the He atom and the excitation rates have a different dependence on the electron energy distribution, these ratios may indicate changes in this distribution. The interpretation of this observation in terms of the change in the electron energy distribution function awaits a more thorough analysis of the population growth and decay processes.

#### B. Temporally Resolved Optical Emission Measurements of Ar and Ar<sup>+</sup>

Temporally resolved observations of neutral Ar at 750.39 nm and Ar<sup>+</sup> at 434.81 nm were accomplished in a pulse counting mode using a TAC and an MCA shown in Figure 2. The TAC converts the time between the start of an rf cycle and the arrival of a photon pulse to a proportional voltage. This voltage is digitized by an MCA with

512 channels and a total acquisition time of 200 ns, thus giving a time resolution per channel of approximately 0.4 ns. The time history of both emission line signals were recorded with respect to the same time on the voltage waveform, therefore their relative phases may be compared.

In an optically thin medium the optical emission intensity per unit time in  $4\pi$  steradians from a transition between two levels is given by,

$$I = n_u A_{ul} h \nu_{ul} \quad (1)$$

where  $n_u$  is the upper state density,  $A_{ul}$  is the atomic transition probability,<sup>10</sup>  $h$  is Plank's constant and  $\nu_{ul}$  is the frequency of the transition. Figures 7 and 8 show, respectively, the temporal evolution of Ar and Ar<sup>+</sup> as a function of the distance above the powered electrode. The plot of the Ar<sup>+</sup> line shows a significant concentrations of ions near the powered electrode and as the distance between the electrodes is scanned the temporal evolution of the ion excited state density shows a significant distortion from sinusoidal. This is not observed in the Ar line. Here the neutral atom excited state density is very small near the powered electrode (the dark space) then rises abruptly after a few mm into a very bright region (the sheath) and decays more rapidly toward the grounded electrode. Also the neutral excited state density does not show any significant non-sinusoidal temporal evolution as does the ion excited state density. The Ar<sup>+</sup> signal has a much smaller signal-to-noise ratio than the neutral Ar which accounts for some of the bumpy structure in Figure 8. The interpretation of these temporally resolved optical emission signals requires the inclusion of many atomic processes. If one assumes the simple collisional-radiative model<sup>9,11</sup> of the plasma processes, then the population growth and decay processes may be assessed.

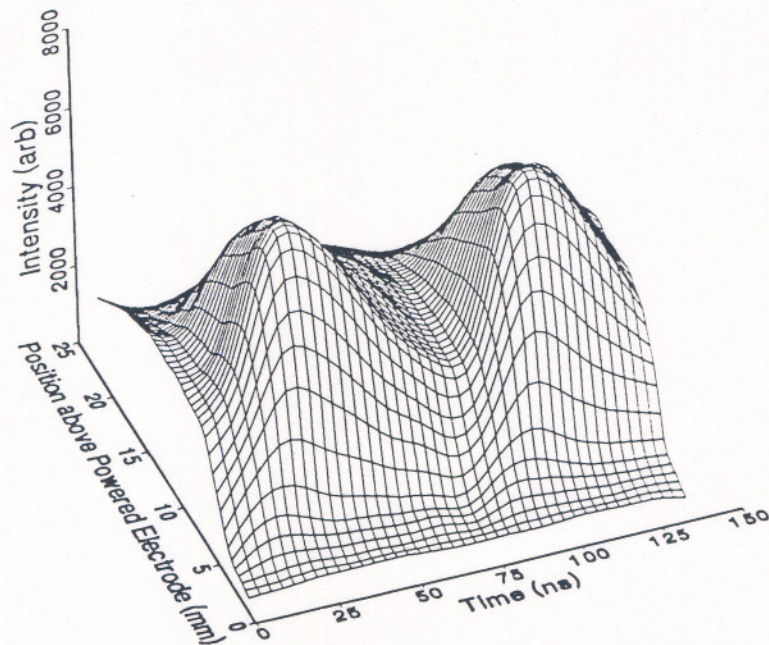


Figure 7. Optical emission measurements of the spatial profile and temporal evolution of the Ar 750.39 nm emission line. The distance between the electrodes is 25.4 mm and the period of the 13.56 MHz RF is 73.7 ns. The pressure of pure Ar is 13.33 Pa.

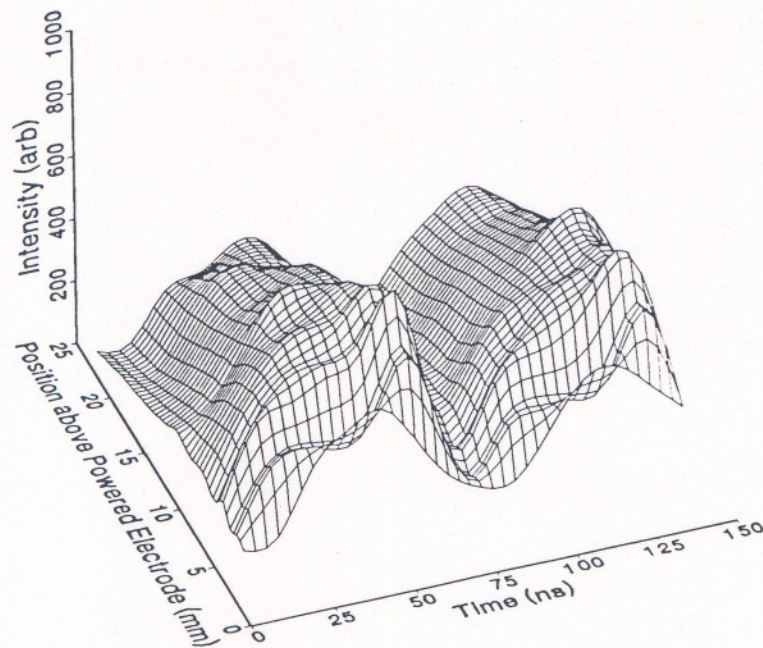


Figure 8. Optical emission measurements of the spatial profile and temporal evolution of the  $\text{Ar}^+$  434.81 nm emission line. The distance between the electrodes is 25.4 mm and the period of the 13.56 MHz RF is 73.7 ns. The pressure of pure Ar is 13.33 Pa.

### C. Spatially Resolved Optical Emission Measurements of Ar

One of the most desirable characteristics of a plasma processing device is to have a well known density profile of the plasma constituents, e.g. a constant radial ion distribution for plasma etching. To investigate the effect of changes in plasma parameters on the radial Ar emission profile, the horizontal distribution of neutral Ar line at 415.86 nm was observed in a pure Ar plasma as a function of pressure. This line was chosen because its emission intensity was much weaker than the stronger Ar emission lines; therefore radiation trapping was not a factor in the analysis. The plasma was scanned at the electrode midplane in a direction parallel to the electrode surfaces by moving the optical table supporting the spectroscopic apparatus horizontally. This scan was then inverted into a radial distribution of the optical emission signal by the Abel integral process.<sup>3,4</sup> The normalized signal of the data as well as the Abel inverted results are presented in Figure 9. The extent of the electrodes is also indicated for comparison. As can be seen the Abel inverted profiles show a substantial difference from the horizontally scanned data as the pressure increases. Also the plasma extends outside the electrode region. These results indicate at lower pressures the plasma density profiles can be expected to be the most uniform.

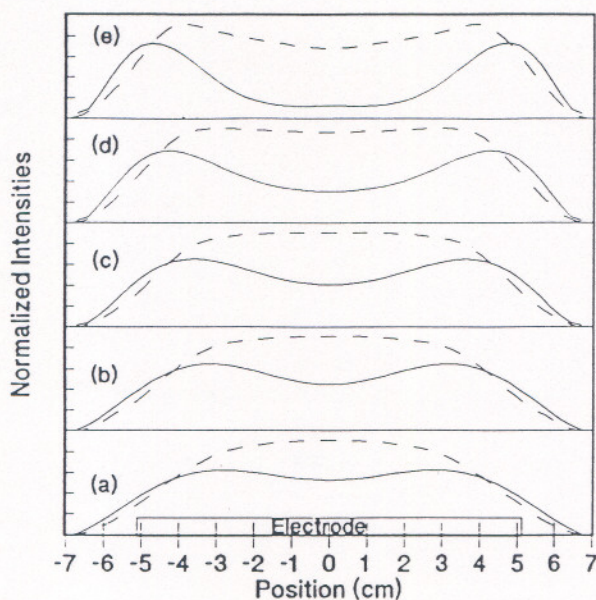


Figure 9. Abel inverted radial emission profiles of the Ar 415.86 nm emission line (solid) and the normalized horizontal emission intensity (dashed) for (a) 6.67, (b) 13.33, (c) 33.33, (d) 66.66, and (e) 133.32 Pa pressures. The electrode limits are indicated.

#### D. Energy Analyzed Mass Spectrometry

Shown in Figure 10 are the ion kinetic energy distributions for  $\text{Ar}^+$  produced in an argon discharge as a function of the probe distance,  $d$ , from the edge of the electrodes. For small  $d$  the distributions exhibit a periodic structure similar to that observed previously for ion energy distributions sampled through the grounded electrode of parallel plate reactors.<sup>8,12,13</sup> This is expected since a sheath develops around the grounded cone as it moves closer to the electrodes thus suggesting that the cone behaves as an extension to the grounded electrode. The observed structure has been attributed to modulation effects associated with  $\text{Ar}^+$  formation by resonant charge transfer in the sheath.<sup>12</sup> As the distance between the probe aperture and the electrodes increases, the structure disappears due to the diminishing influence of the probe in defining a sheath region near the aperture.

Ions sampled in the present configuration obtain most of their kinetic energy from traversing the sheath potential as they are accelerated from the bulk plasma toward the grounded surface. The maximum observed kinetic energy of an ion therefore provides an indication of the sheath potential if the energy distribution has not been severely disturbed by collisions in the sheath or by ions being created in the sheath region. The broad range of energies (0-20 eV) observed for  $\text{Ar}^+$  in Figure 10 indicate that such processes do occur for  $\text{Ar}^+$ . Similar ion kinetic energy distributions are observed for  $\text{Ar}^{++}$  since  $\text{Ar}^{++}$  is formed in the sheath by high energy electron collisions.

Unlike  $\text{Ar}^+$ ,  $\text{Ar}_2^+$  ion kinetic energy distributions (see Figure 11) are narrow and exhibit no secondary structure. This indicates  $\text{Ar}_2^+$  ions are not created in the sheath and the maximum ion energy may be used to estimate the sheath potential.<sup>6</sup> The distributions in Figure 11 are in agreement with previous ion energy distributions for  $\text{Ar}_2^+$  measured by Köhler et al.<sup>6</sup> using a spherical energy analyzer sampling through a

grounded electrode. As  $d$  increases the average energy of the  $\text{Ar}_2^+$  ions decreases due to the influence of inelastic collisions.

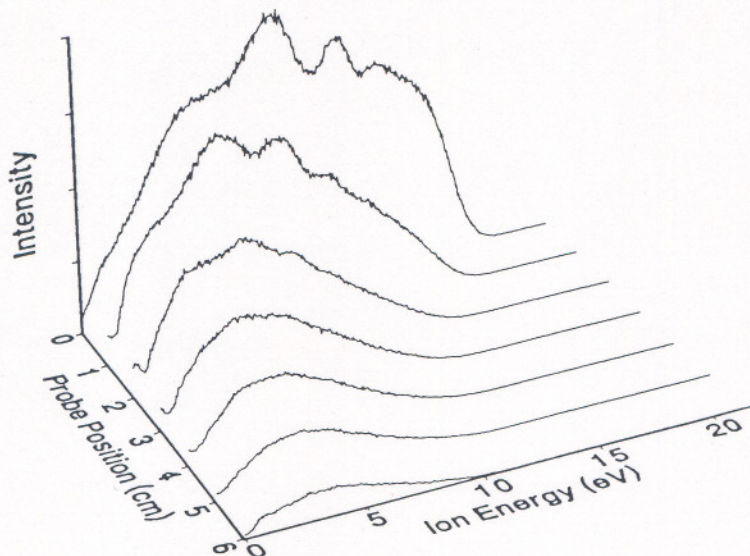


Figure 10.  $\text{Ar}^+$  kinetic energy distributions as a function of probe position for a 13.33 Pa argon plasma with  $V_{pp} = 200$  V.

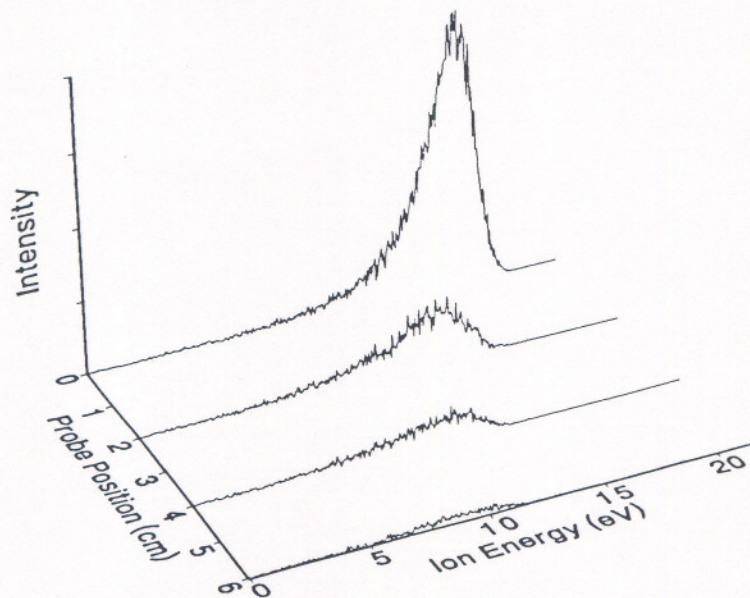


Figure 11.  $\text{Ar}_2^+$  kinetic energy distributions as a function of probe position for a 13.33 Pa argon plasma with  $V_{pp} = 200$  V.

## IV. CONCLUSIONS

A substantial amount of information about an rf plasma may be derived using optical emission diagnostics and ion energy analyzed mass spectrometry. Optical emission spectroscopy provides a direct means of monitoring the spatial profiles of the density of plasma atoms and ions. Temporally resolved measurements allow one to deduce information about the evolution of these constituent densities present in the plasma. Investigation of the variations of different transitions allows one to monitor the effects of electrons as the plasma conditions are changed. Mass spectrometry with kinetic energy analysis can determine relative ion fluxes, monitor sheath potentials, and provide information about the interactions of ions and neutrals in the sheath region.

While a great amount of information is provided by these two methods, much of the data becomes extremely complex for plasmas on commercial etching reactors. Significant research must still be done in order to determine which aspects of the data are of direct importance in monitoring the plasma conditions and/or the etching process. An extension of the results presented here to systems containing etching gases and to more complex etching instrumentation is also required.

## ACKNOWLEDGEMENTS

This work has been partially supported by SEMATECH.

## REFERENCES

1. J. R. Roberts, J. K. Olthoff, R. J. Van Brunt, and J. R. Whetstone, Advanced Techniques for Integrated Circuit Processing, 1392, 428, (Society for Photo-Optical Instrumentation Engineers, 1991).
2. A. Picard, G. Turban and B. Grollean, *J. Phys. D*, **19**, 991 (1986).
3. M. P. Freeman and S. Katz, *J. Opt. Soc. Am.* **50**, 826 (1960) and *J. Opt. Soc. Am.* **53**, 1172 (1963)
4. S. I. Herlitz, *Ark. Fys.* **23**, 571 (1963).
5. H. Z. Sar-el, *Rev. Sci. Inst.*, **38**, 1210 (1967).
6. K. Köhler, J. W. Coburn, D. E. Horne, and E. Kay, *J. Appl. Phys.*, **57**, 59 (1985).
7. W. M. Greene, M. A. Hartney, W. G. Oldham, and D. W. Hess, *J. Appl. Phys.*, **63**, 1367 (1988).
8. M. F. Toups and D. W. Ernie, *J. Appl. Phys.* **68**, 6125 (1990).
9. R. W. P. McWhirter, Plasma Diagnostic Techniques, edited by R. H. Huddelstone and S. L. Leonard (Academic Press, New York, 1965), Chap. 5, pp 201-264.
10. W. L. Wiese, M. W. Smith, and B. M. Miles, Atomic Transition Probabilities, Natl. Stand. Ref. Data Ser., Natl. Bur. Stand. (US) **22** Vol.II (1969).
11. C. Böhm and J. Perrin, *J. Phys. D*. **24**, 865 (1991).
12. C. Wild and P. Koidl, *J. Appl. Phys.*, **69**, 2909 (1991).
13. J. Liu, G. L. Huppert, and H. H. Sawin, *J. Appl. Phys.*, **68**, 3916 (1990).
14. L. J. Overzet, J. H. Beberman, and J. T. Verdegem, *J. Appl. Phys.*, **66**, 1622 (1989).
15. C. W. Jurgensen, *J. Appl. Phys.*, Vol. **64**, 590 (1988).

\* The identification of commercial materials and their sources is made to describe the experiment adequately. In no case does this identification imply recommendation by the National Institute of Standards and Technology, nor does it imply that the instrument is the best available.